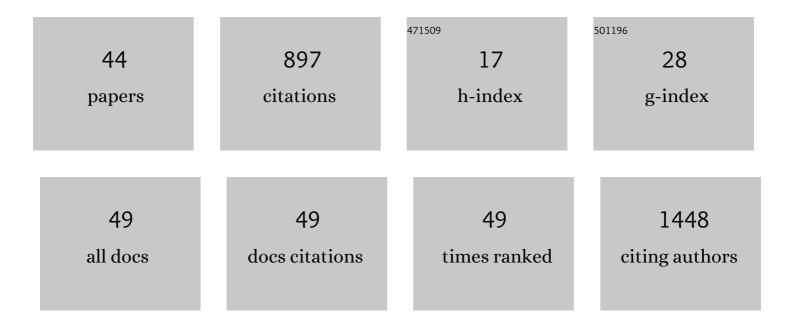
Tamas Varga

List of Publications by Year in descending order

Source: https://exaly.com/author-pdf/5025543/publications.pdf Version: 2024-02-01



TAMAS VADCA

#	Article	IF	CITATIONS
1	Soil pore network response to freeze-thaw cycles in permafrost aggregates. Geoderma, 2022, 411, 115674.	5.1	30
2	The behavior of iodine in stabilized granular activated carbon and silver mordenite in cementitious waste forms. Journal of Environmental Radioactivity, 2022, 244-245, 106824.	1.7	2
3	In-situ X-ray and visual observation of foam morphology and behavior at the batch-melt interface during melting of simulated waste glass. Ceramics International, 2022, 48, 7975-7985.	4.8	6
4	Tuning the Charge and Hydrophobicity of Graphene Oxide Membranes by Functionalization with Ionic Liquids at Epoxide Sites. ACS Applied Materials & Interfaces, 2022, 14, 19031-19042.	8.0	6
5	Ripples at edges of blooming lilies and torn plastic sheets. Biophysical Journal, 2022, 121, 2389-2397.	0.5	1
6	Effects of Microbial-Mineral Interactions on Organic Carbon Stabilization in a Ponderosa Pine Root Zone: A Micro-Scale Approach. Frontiers in Earth Science, 2022, 10, .	1.8	1
7	Microstructural evolution and precipitation in γ-LiAlO2 during ion irradiation. Journal of Applied Physics, 2022, 131, .	2.5	6
8	Behavior of iodate substituted ettringite during aqueous leaching. Applied Geochemistry, 2021, 125, 104863.	3.0	6
9	Through a glass darkly: In-situ x-ray computed tomography imaging of feed melting in continuously fed laboratory-scale glass melter. Ceramics International, 2021, 47, 15807-15818.	4.8	11
10	Soil texture and environmental conditions influence the biogeochemical responses of soils to drought and flooding. Communications Earth & Environment, 2021, 2, .	6.8	35
11	Understanding the Electronic Structure Evolution of Epitaxial LaNi _{1–<i>x</i>} Fe _{<i>x</i>} O ₃ Thin Films for Water Oxidation. Nano Letters, 2021, 21, 8324-8331.	9.1	31
12	Spatial access and resource limitations control carbon mineralization in soils. Soil Biology and Biochemistry, 2021, 162, 108427.	8.8	7
13	Competitive TcO4–, IO3–, and CrO42– Incorporation into Ettringite. Environmental Science & Technology, 2021, 55, 1057-1066.	10.0	11
14	Evolution of metastable phases during Mg metal corrosion: An <i>in situ</i> cryogenic x-ray photoelectron spectroscopy study. Journal of Vacuum Science and Technology A: Vacuum, Surfaces and Films, 2021, 39, .	2.1	3
15	Polymer-cement composites with adhesion and re-adhesion (healing) to casing capability for geothermal wellbore applications. Cement and Concrete Composites, 2020, 107, 103490.	10.7	9
16	Immobilizing Pertechnetate in Ettringite via Sulfate Substitution. Environmental Science & Technology, 2020, 54, 13610-13618.	10.0	20
17	Metal–Organic Framework–Polyacrylonitrile Composite Beads for Xenon Capture. ACS Applied Materials & Interfaces, 2020, 12, 45342-45350.	8.0	25
18	Electric field stimulates production of highly conductive microbial OmcZ nanowires. Nature Chemical Biology, 2020, 16, 1136-1142.	8.0	112

TAMAS VARGA

#	Article	IF	CITATIONS
19	In situ characterization of foam morphology during melting of simulated waste glass using x-ray computed tomography. Ceramics International, 2020, 46, 17176-17185.	4.8	15
20	Calcareous organic matter coatings sequester siderophores in alkaline soils. Science of the Total Environment, 2020, 724, 138250.	8.0	14
21	Probing the Radial Chemistry of Getter Components in Light Water Reactors via Controlled Electrochemical Dissolution. ACS Omega, 2020, 5, 13578-13587.	3.5	1
22	An electrochemical technique for controlled dissolution of zirconium based components of light water reactors. RSC Advances, 2019, 9, 1869-1881.	3.6	1
23	Chromate Effect on lodate Incorporation into Calcite. ACS Earth and Space Chemistry, 2019, 3, 1624-1630.	2.7	16
24	Unraveling the mysterious failure of Cu/SAPO-34 selective catalytic reduction catalysts. Nature Communications, 2019, 10, 1137.	12.8	99
25	Insights into the physical and chemical properties of a cement-polymer composite developed for geothermal wellbore applications. Cement and Concrete Composites, 2019, 97, 279-287.	10.7	22
26	Inorganic Ba–Sn nanocomposite materials for sulfate sequestration from complex aqueous solutions. Environmental Science: Nano, 2018, 5, 890-903.	4.3	5
27	Creation and Ordering of Oxygen Vacancies at WO _{3â~î´} and Perovskite Interfaces. ACS Applied Materials & Interfaces, 2018, 10, 17480-17486.	8.0	29
28	Tuning piezoelectric properties through epitaxy of La2Ti2O7 and related thin films. Scientific Reports, 2018, 8, 3037.	3.3	15
29	Preâ€Viking Swedish hillfort glass: A prospective longâ€term alteration analogue for vitrified nuclear waste. International Journal of Applied Glass Science, 2018, 9, 540-554.	2.0	13
30	The Ability of Soil Pore Network Metrics to Predict Redox Dynamics is Scale Dependent. Soil Systems, 2018, 2, 66.	2.6	16
31	Controlling the structure and ferroic properties of strained epitaxial NiTiO3 thin films on sapphire by post-deposition annealing. Thin Solid Films, 2018, 662, 47-53.	1.8	3
32	Coupled Lattice Polarization and Ferromagnetism in Multiferroic NiTiO ₃ Thin Films. ACS Applied Materials & Interfaces, 2017, 9, 21879-21890.	8.0	18
33	Phase transformation kinetics in rolled U-10Âwt. % Mo foil: Effect of post-rolling heat treatment and prior γ-UMo grain size. Journal of Nuclear Materials, 2017, 496, 215-226.	2.7	20
34	What can we learn from in-soil imaging of a live plant: X-ray Computed Tomography and 3D numerical simulation of root-soil system. Rhizosphere, 2017, 3, 259-262.	3.0	12
35	Pore-Engineered Metal–Organic Frameworks with Excellent Adsorption of Water and Fluorocarbon Refrigerant for Cooling Applications. Journal of the American Chemical Society, 2017, 139, 10601-10604.	13.7	128
36	Molecular and Microscopic Insights into the Formation of Soil Organic Matter in a Red Pine Rhizosphere. Soils, 2017, 1, 4.	1.0	12

TAMAS VARGA

#	Article	IF	CITATIONS
37	Inorganic tin aluminophosphate nanocomposite for reductive separation of pertechnetate. Environmental Science: Nano, 2016, 3, 1003-1013.	4.3	24
38	RedOx-controlled sorption of iodine anions by hydrotalcite composites. RSC Advances, 2016, 6, 76042-76055.	3.6	23
39	Extracting Metrics for Three-dimensional Root Systems: Volume and Surface Analysis from In-soil X-ray Computed Tomography Data. Journal of Visualized Experiments, 2016, , .	0.3	2
40	Strain-Dependence of the Structure and Ferroic Properties of Epitaxial NiTiO ₃ Thin Films Grown on Different Substrates. Advances in Condensed Matter Physics, 2015, 2015, 1-9.	1.1	7
41	Strain-dependence of the structure and ferroic properties of epitaxial Ni1â^'xTi1â^'yO3 thin films grown on sapphire substrates. Thin Solid Films, 2015, 578, 113-123.	1.8	7
42	Strain Accommodation by Facile WO ₆ Octahedral Distortion and Tilting during WO ₃ Heteroepitaxy on SrTiO ₃ (001). ACS Applied Materials & Interfaces, 2014, 6, 14253-14258.	8.0	29
43	Coexistence of weak ferromagnetism and polar lattice distortion in epitaxial NiTiO3 thin films of the LiNbO3-type structure. Journal of Vacuum Science and Technology B:Nanotechnology and Microelectronics, 2013, 31, 030603.	1.2	17
44	Epitaxial growth of NiTiO3 with a distorted ilmenite structure. Thin Solid Films, 2012, 520, 5534-5541.	1.8	24